AGU PUBLICATIONS

JGR

Journal of Geophysical Research: Space Physics

RESEARCH ARTICLE
10.1002/2015JA021835

**Key Points:**
- Extremely intense substorms/ supersubstorms are often isolated events and are not obvious statistical fluctuations of the geomagnetic indices
- Supersubstorm occurrence and intensity have no obvious relationship with geomagnetic storm intensity
- Supersubstorms exhibit annual variation with peak occurrence during spring in SC 22 and fall in SC 23

**Correspondence to:**
R. Hajra,
rajkumarhajra@yahoo.co.in

**Citation:**
Hajra, R., B. T. Tsurutani, E. Echer, W. D. Gonzalez, and J. W. Gjerloev (2016), Supersubstorms (SML $< -2500$ nT): Magnetic storm and solar cycle dependences, *J. Geophys. Res. Space Physics*, *121*, doi:10.1002/2015JA021835.

Received 20 AUG 2015
Accepted 4 AUG 2016
Accepted article online 9 AUG 2016



# Supersubstorms (SML $< -2500$ nT): Magnetic storm and solar cycle dependences

**Rajkumar Hajra[1,2], Bruce T. Tsurutani[3], Ezequiel Echer[1], Walter D. Gonzalez[1], and Jesper W. Gjerloev[4,5]**

[1]Instituto Nacional de Pesquisas Espaciais, São José dos Campos, São Paulo, Brazil, [2]Now at Laboratoire de Physique et Chimie de l'Environnement et de l'Espace, CNRS, Orléans, France, [3]Jet Propulsion Laboratory, California Institute of Technology, Pasadena, California, USA, [4]The Johns Hopkins University Applied Physics Laboratory, Laurel, Maryland, USA, [5]Birkeland Center, University of Bergen, Bergen, Norway

**Abstract** We study extremely intense substorms with SuperMAG *AL* (SML) peak intensities $< -2500$ nT ("supersubstorms"/SSSs) for the period from 1981 to 2012. The SSS events were often found to be isolated SML peaks and not statistical fluctuations of the indices. The SSSs occur during all phases of the solar cycle with the highest occurrence (3.8 year$^{-1}$) in the descending phase. The SSSs exhibited an annual variation with equinoctial maximum altering between spring in solar cycle 22 and fall in solar cycle 23. The occurrence rate and strength of the SSSs did not show any strong relationship with the intensity of the associated geomagnetic storms. All SSS events were associated with strong southward interplanetary magnetic field $B_s$ component. The $B_s$ fields were part of interplanetary magnetic clouds in 46% and of interplanetary sheath fields in 54% of the cases. About 77% of the SSSs were associated with small regions of very high density solar wind plasma parcels or pressure pulses impinging upon the magnetosphere. Comments on how SSS events may cause power outages at Earth are discussed at the end of the paper.

## 1. Introduction

The occurrence of magnetospheric substorms is the dominant and fundamental mechanism of global energy deposition into the Earth's magnetosphere and ionosphere [*Akasofu*, 1964; *Rostoker et al*., 1980; *Baker et al*., 1996; *Liou et al*., 2001; *Østgaard et al*., 2005]. The temporal evolution of auroras caused by precipitating energetic particles into the ionosphere is very similar to the sequence originally proposed by *Akasofu* [1964]. The name "substorm" comes from the then belief that substorms were the integral part of magnetic storms [*Akasofu*, 1968, 2004; *Hamilton et al*., 1988; *Daglis et al*., 1994; *Gonzalez et al*., 1994], the latter of which are cases of even larger magnetospheric and ionospheric energy dissipation. However, it is well known that substorms can occur independently of storms [e.g., *Tsurutani and Meng*, 1972; *Iyemori and Rao*, 1996; *Tsurutani et al*., 2004a]. A series of substorms and convection events called HILDCAAs (high-intensity long-duration continuous *AE* activity events, *Tsurutani and Gonzalez* [1987]) occur outside of magnetic storm main phases [*Hajra et al*., 2013, 2014a, 2014b, 2014c, 2015a, 2015b]. Magnetic storms have also been detected without substorms [*Tsurutani et al*., 2003a, 2004b].

The ultimate energy driving magnetospheric substorms and storms is the solar wind. When the interplanetary magnetic field (IMF) turns southward, magnetic reconnection between the IMF and the Earth's magnetopause field [*Dungey*, 1961] leads to energy transfer into the magnetotail/magnetosphere [e.g., *Tsurutani and Meng*, 1972; *Gonzalez et al*., 1994; *Echer et al*., 2008a].

It is the purpose of this paper to study various facets of extreme substorms from 1981 to 2012, approximately three solar cycles. We will call these very intense substorms "supersubstorms" or SSS events for shorthand. We arbitrarily chose a threshold of SuperMAG *AL* (SML) peak intensity $< -2500$ nT for the SSS events. The SML indices will be defined and described in more detail in section 2. The events are important not only for understanding the physical processes of the events themselves, but SSSs are potential causes for power outages [see *Huttunen et al*., 2008; *Beggan et al*., 2013; *Schrijver et al*., 2014; *Tsurutani et al*., 2015]. We will attempt to identify the interplanetary causative features and the seasonal and solar cycle dependences of such extreme events. This is the first time that such a study of this type has been carried out.

## 2. Database and Methodology

We identified and examined intense substorms using ground-based magnetic observations from 1981 to 2012, from approximately the maximum phase of solar cycle (SC) 21 to the approximate maximum phase of SC 24. In this study substorms were identified from the SML index which is a generalization of the well-known *AL* index [*Davis and Sugiura*, 1966]. *AL*, a proxy of the westward auroral electrojet, is derived based on observations from 12 geomagnetic stations (~60°N–70°N). It is reported to be insufficient for auroral activities located at very high or very low latitudes [e.g., *Rostoker*, 1972; *Kamide and Akasofu*, 1983; *Ahn et al*., 2000].

The SML index is constructed from ground magnetometer data from the SuperMAG sites including not only the standard *AL* magnetometer sites but also higher-latitude and lower latitude stations as well. The SuperMAG network (http://supermag.jhuapl.edu/) consists of more than 300 ground-based magnetometers operated by a variety of worldwide organizational and national agencies. The data grid covers midlatitude ionospheric currents which occur during intense geomagnetic storm activity when auroras and their associated currents move equatorward of the nominal (~60° to 70° magnetic latitude) auroral zone, and also high-latitude stations that can cover auroral activity that occurs at latitudes higher than the nominal auroral zone for weak geomagnetic activity intervals. Detailed descriptions of the SuperMAG project and the identification of substorms from the SML indices are given in *Gjerloev* [2009, 2012] and *Newell and Gjerloev* [2011a, 2011b].

In the present study, a substorm is defined as an interval of increased energy dissipation to the auroral ionosphere, determined by the westward auroral electrojet index (SML) [*Rostoker et al*., 1980]. According to a simple algorithm suggested by *Newell and Gjerloev* [2011a], a substorm onset is identified by (i) a sharp decrease in the SML index, more than 45 nT in 3 min, that leads to a negative bay development and (ii) maintenance of SML below $-100$ nT of the initial value for the subsequent 26 min. It may be mentioned that in the original paper on substorms [*Akasofu*, 1964], Akasofu described a generic sequence of auroral phenomena. At that time there was no discussion on energy loading/unloading scenario. *Newell and Gjerloev* [2011a] have followed this original definition in identifying substorms. The identified substorms then were compared with those identified by the Polar Ultraviolet Imager (UVI). It was shown that for the 1997–1998 period, the SML index is ~50% more likely to identify an onset seen by the Polar UVI than is the *AL* index. We refer the reader to the list of the substorms identified by their study (http://supermag.jhuapl.edu/substorms/). For the present study, we will focus on substorms with peak SML values $< -2500$ nT. This arbitrary threshold intensity was chosen to identify extremely intense substorms, supersubstorms or SSS events. Seventy-four such events have been identified in the interval from 1981 to 2012. We studied Polar UVI images for all the events. Intense auroral expansions were recorded during the events whenever nighttime UVI observations were available. A list of the SSS events may be available upon request.

The threshold of SML $< -2500$ nT was an arbitrary one. Other thresholds were used with the same results. We do not show this for brevity. For a comparison to the SML index, we also made a similar search based on the *AL* $< -2500$ nT. The same events were identified by both SML and *AL* indices, and specific examples will be shown in the body of the text.

The geomagnetic indices *Dst* (1 h), *SYM-H* (1 min), and *AL* (1 min) were obtained from the World Data Center for Geomagnetism, Kyoto, Japan (http://wdc.kugi.kyoto-u.ac.jp/). We used the 1 h *Dst* index for classification of the geomagnetic storms according to *Dst* peak strength [*Gonzalez et al*., 1994; *Echer et al*., 2011a]. In the remainder of the paper, we use higher time-resolution (1 min) *SYM-H* data to identify the instantaneous geomagnetic storm conditions.

Solar wind/interplanetary data at 1 min time resolution were obtained from the OMNI website (http://omniweb.gsfc.nasa.gov/). The OMNI interplanetary data had been already time adjusted to take into account the solar wind propagation time from the spacecraft to the bow shock, so no further adjustments to the interplanetary data were made in this study (see http://omniweb.gsfc.nasa.gov/html/omni_min_data.html). The yearly average $F_{10.7}$ solar flux data (http://www.drao.nrc.ca/icarus) were used to identify solar cycle phases.

## 3. Results

### 3.1. SSS Event Case Study

Figure 1 shows an example of solar wind/interplanetary and geomagnetic conditions associated with two SSS events identified by the SML index on 11 April 2001. For comparison, we also plot the *AL* index during the SSS

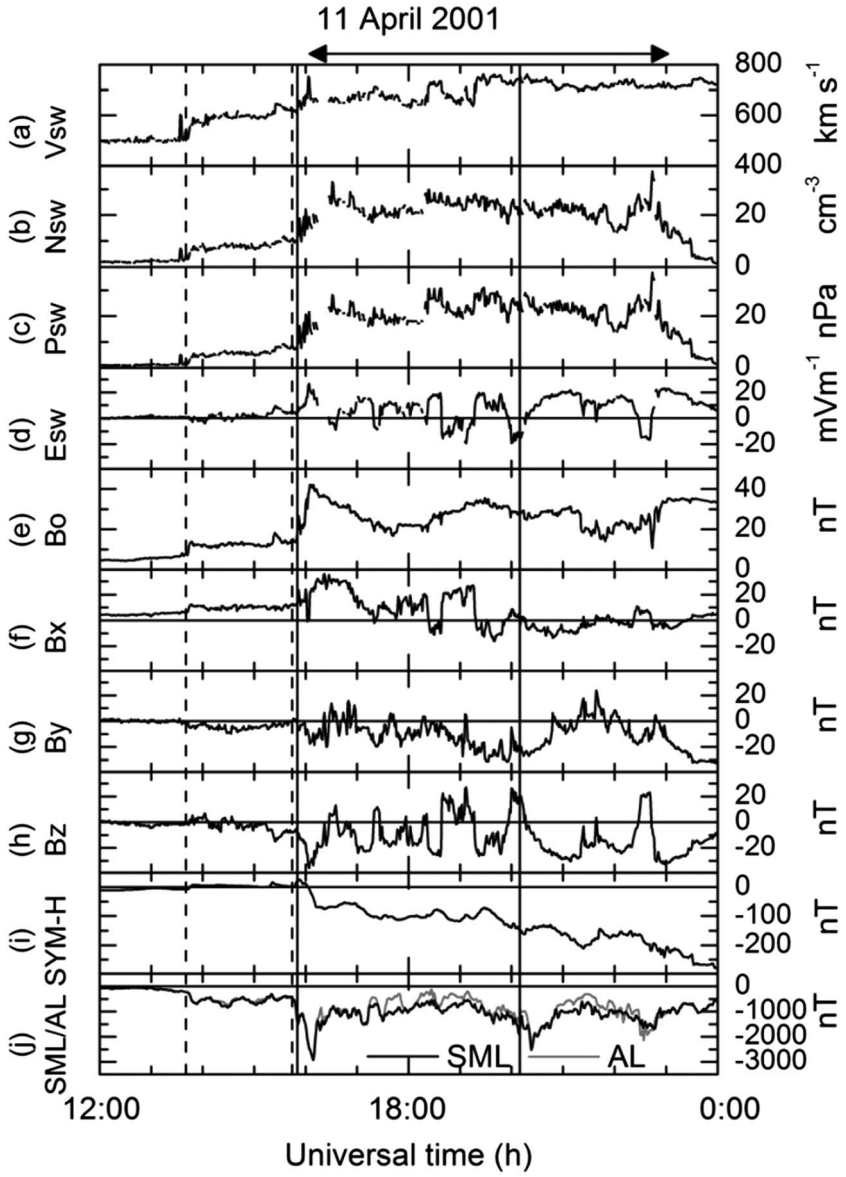


**Figure 1.** Interplanetary and geomagnetic parameters during two SSS events occurring on 11 April 2001. From top to bottom, the panels show (a) the solar wind speed ($V_{sw}$ in km s$^{-1}$), (b) the density ($N_{sw}$ in cm$^{-3}$), (c) the plasma ram pressure ($P_{sw}$ in nPa), (d) the interplanetary dawn-to-dusk electric field ($E_{sw}$ in mV$^{-1}$), (e) the interplanetary magnetic field (IMF) magnitude ($B_o$ in nT), (f) the $B_x$ (nT), (g) $B_y$ (nT) and (h) $B_z$ (nT) components in GSM coordinates, (i) the *SYM-H* (nT), (j) the SML (nT) (black) and the *AL* (nT), indices (gray). Onsets of the SSS events are indicated by vertical solid lines. The vertical dashed lines show the two interplanetary shocks. The horizontal arrow in the top shows the interplanetary sheath region. The two SSS events took place in the main phase of a superstorm (peak *SYM-H* = −280 nT).

events. The first SSS event started at ~1553 UT, as indicated by a sharp decrease in SML (*AL*). The SSS had a peak SML intensity of −2923 nT (a peak *AL* of −2903 nT) at ~1609 UT. The SSS event continued until ~1633 UT giving it a duration of ~40 min. The SSS event was an "isolated" event with a much higher SML peak than values either before or after the event. The instantaneous *SYM-H* was ~ +15 nT at the SSS onset. At the SSS peak intensity, *SYM-H* was −68 nT.

The second SSS event took place from ~2016 UT to 2051 UT and had a duration of ~35 min. It is also an isolated event with its peak intensity considerably higher than either prior to the event or after the event. It had a peak SML intensity of −2524 nT (a peak *AL* of −2339 nT) at ~2023 UT. During this SSS event, the instantaneous *SYM-H* was −160 nT.

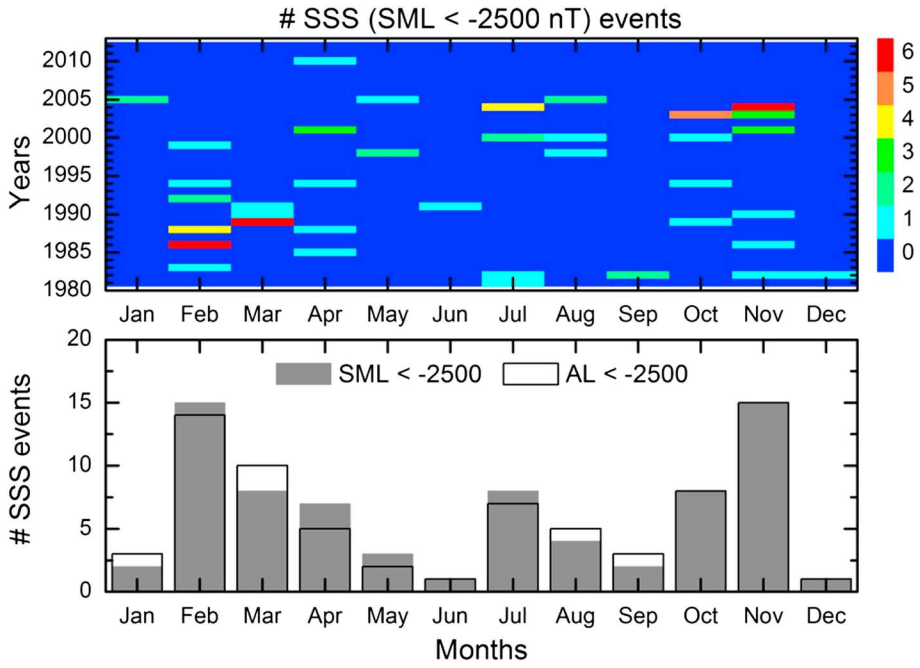


**Figure 2.** (top) Two-dimensional plot of the number of SSS events (SML $< -2500$ nT) in each month of the year for the interval of study from 1981 to 2012. The values of different colors are given in the legend at the right. (bottom) Monthly number of SSS events summed over the entire period of observation. The gray and empty histograms show SML $< -2500$ nT and *AL* $< -2500$ nT events, respectively.

Both of the SSS events occurred in the main phase of a "superstorm" which had a peak *SYM-H* intensity of ~ −280 nT (peak *Dst* = −271 nT). Superstorms have been defined as those with *Dst* ≤ −250 nT [*Tsurutani et al*., 1992a; *Echer et al*., 2008b]. The time differences of the two SSS peaks from the magnetic storm peak were ~7.8 h and ~3.6 h, respectively. Thus, although the SSS events were associated with the main phase of a superstorm, they occurred well ahead of the storm peak intensity. This is an important point and will be discussed again later.

The interplanetary event that caused the two SSS events appears to be part of an interplanetary sheath [*Tsurutani et al*., 1988]. The sheath starts at the (second) shock, ~1550 UT and continues until the start of a magnetic cloud (MC) at ~2200 UT [see *Echer et al*., 2008a]. The sheath region is shown by a horizontal arrow on the top of Figure 1. The sheath is characterized by multiple IMF $B_z$ changes. The solar wind speed reached a maximum of ~760 km s$^{-1}$ at ~1927 UT. This point in time is between the first and second SSS events.

There was a southward turning of IMF $B_z$ ~39 min prior to the first SSS initiation. The solar wind plasma preconditions were as follows: the solar wind speed $V_{sw}$ was ~650 km s$^{-1}$, plasma density $N_{sw}$ ~11 cm$^{-3}$, and ram pressure $P_{sw}$ ~9 nPa. For the second SSS event, the onset corresponds to a southward turning of the IMF $B_z$ and the onset of a dawn-to-dusk directed $E_{sw}$. At onset, the $V_{sw}$ was ~744 km s$^{-1}$, $N_{sw}$ ~23 cm$^{-3}$, and $P_{sw}$ ~24 nPa.

Two interplanetary fast forward shocks were detected at ~1341 and ~1550 UT (shown by vertical dashed lines). The second shock can be identified by a jump in $V_{sw}$ from ~610 to 750 km s$^{-1}$, in $N_{sw}$ from ~9.5 to 22.2 cm$^{-3}$, and in $B_o$ from ~14.3 to 42.1 nT. The ram pressure $P_{sw}$ jumped from ~7.1 to 21.6 nPa across the shock, a threefold increase. The shock normal direction was determined using the *Abraham-Schrauner* [1972] method, and then the Rankine-Hugoniot conservation equations were used to get the shock speed [*Smith*, 1985; *Tsurutani and Lin*, 1985; *Tsurutani et al*., 2011a]. The shock was found to have a magnetosonic Mach number of 2.7 and a shock normal angle of 49° relative to the upstream magnetic field. This second shock "pressure pulse" is time coincident with the first SSS event onset. The second SSS event did not seem to have any associated pressure pulse.

### 3.2. SSS Seasonal Dependence

Figure 2 shows the distribution of all 74 SSS events detected during the interval 1981–2012. The events were found to be isolated peak occurrences in SML indices. About 63% of the SSS events had peak SML values

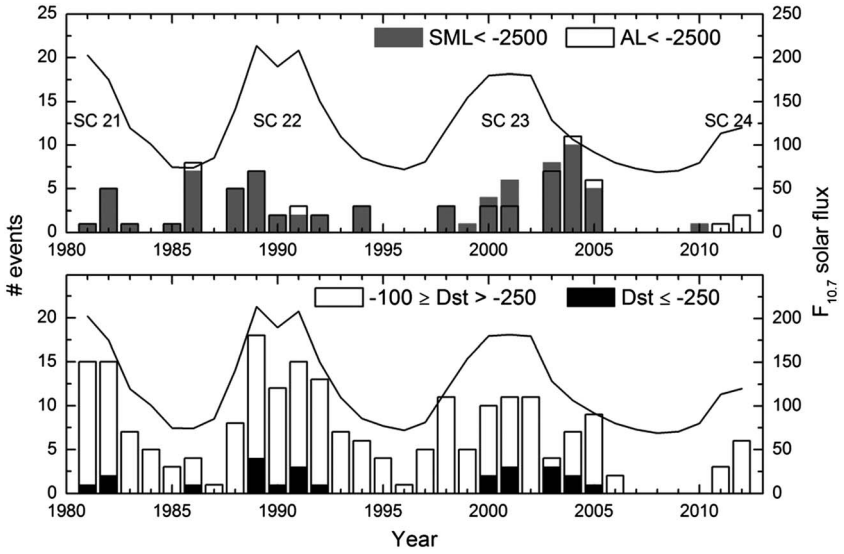


**Figure 3.** Gray histograms in the upper panel show the yearly number of SSS events (SML $< -2500$ nT) during the period 1981–2012. The empty histograms show the $AL < -2500$ nT events. These are the same as in Figure 2. The number of geomagnetic storms of different intensities (*Dst*) are shown by the histograms in Figure 3 (bottom). The different storm intensities are $-100\,\text{nT} \geq Dst > -250$ nT (intense) and $Dst \leq -250$ nT (super intense). The continuous lines (secondary *y* axis, legend on the right) in both panels are the yearly average $F_{10.7}$ solar flux. The solar cycle (SC) numbers are indicated in Figure 3 (top).

separated by more than 6 h. Fifteen percent of the SSS events were separated by ~1 to 6 h, and ~22% of the events were separated by less than 1 h.

Figure 2 (top) shows the distribution of all events for each month in the interval 1981–2012 in a two-dimensional (month-year) contour plot. The monthly number of the events summed over the entire period of observation is given in Figure 2 (bottom). In this panel, we show the $AL < -2500$ nT events as well for a comparison with the SSS events (SML $< -2500$ nT). Both indices are found to result in an overall similar seasonal variation. Figure 2 (bottom) indicates that the SSS events exhibit an approximate "semiannual" variation with peak occurrences during February and November with a secondary peak during July. However, Figure 2 (top) shows that there is not a single year with two seasonal peaks. The dominant pattern is one of an annual variation. A close look reveals a shift of the SSS occurrence peak from SC 22 spring to SC 23 fall. The largest numbers of SSS events occur in two time intervals: during February and March in 1985 to 1988 and September and October in 2003 and 2004. Clearly, the semiannual variation presented in Figure 2 (bottom) is an artifact resulting from superposition of years with a dominant annual variation with opposite equinoctial maxima. The same conclusion was drawn by *Mursula et al*. [2011] based on the statistical study of substorm mean amplitude identified by the IMAGE network. It was suggested to be related to the hemispherically asymmetric distribution of the solar magnetic fields that change systematically between the solar cycles in ~22 years [e.g., *Schwabe and Schwabe*, 1844; *Zieger and Mursula*, 1998; *Hathaway*, 2010]. Favorable SSS occurrences during the winter and the summer solstices, as prominent from the average pattern (Figure 2, bottom), may indicate possible ionospheric control on SSS occurrence [*Wang and Lühr*, 2007]. Figure 2 (top) indicates the presence of a SSS solar cycle dependence. This will be described in greater detail below.

### 3.3. SSS Solar Cycle Dependence

Figure 3 (top) shows the SSS solar cycle dependence during the period 1981–2012. In this panel we show the $AL < -2500$ nT events as well for a comparison with the SSS events (SML $< -2500$ nT). Both indices are found to exhibit an overall similar solar cycle variation. The $F_{10.7}$ solar flux (in the unit of $10^{-22}\,\text{W m}^{-2}\,\text{Hz}^{-1}$) is given as a solid black line with the scale on the right. The SSS events were detected during all phases of the solar cycle.

We divided the SSS events into four solar cycle phases. The definition of the phases and the results are given in Table 1. The SSSs are found to occur most frequently ($3.8\,\text{year}^{-1}$) during the descending phase of the solar

**Table 1.** SSS Events During Four Phases of the Solar Cycle During 1981–2012

| Solar Cycle Phase | Years | Number of SSSs | SSS/Year |
|---|---|---|---|
| Ascending | 1987–1988, 1998–1999, 2011–2012 | 9 | 1.5 |
| Maximum | 1981, 1989–1991, 2000–2002 | 22 | 3.1 |
| Descending | 1982–1984, 1992–1994, 2003–2005 | 34 | 3.8 |
| Minimum | 1985–1986, 1995–1997, 2006–2010 | 9 | 0.9 |
| Total | 1981–2012 | 74 | 2.3 |

cycle. This statistics is formed mainly from 3 years, 2003–2005 (68% of 34 events) during the descending phase of SC 23. Occurrence during solar maximum (3.1 year$^{-1}$) is comparable to that in the descending phase. The lowest occurrence frequency (0.9 year$^{-1}$) was noted during solar minimum. There were no SSS events during the two solar/geomagnetic minima, 1996–1997, 2008–2009, and the neighboring years of the latter minimum, 2006–2007. This result is consistent with the overall lower geomagnetic/auroral (HILDCAA) activity around the recent solar minimum, discussed by *Tsurutani et al*. [2011b], *Echer et al*. [2011b], and *Hajra et al*. [2013].

For comparison, we study the yearly occurrence of geomagnetic storms of varying intensity: intense ($-100\,\text{nT} \geq Dst > -250\,\text{nT}$) and "super intense" ($Dst \leq -250\,\text{nT}$). This is shown in Figure 3 (bottom). The solar cycle dependence of geomagnetic storms of varying intensity has been previously studied [*Sugiura*, 1980; *Gonzalez and Tsurutani*, 1987; *Gonzalez et al*., 1994; *Chakraborty and Hajra*, 2010; *Hajra et al*., 2010; *Echer et al*., 2008a, 2011a, 2013; *Hajra*, 2011], and we reproduce their results here. While the geomagnetic storms are found to occur during all phases of the solar cycle, peak occurrence of intense storms is concentrated around the $F_{10.7}$ solar cycle peaks. However, an appreciable number of intense storms are noted to occur in the descending phase. For SC 22, these storms exhibit a two-peak distribution, while there are three peaks for SC 23. Superstorms are found to occur mostly during solar maximum [*Gonzalez et al*., 1990; *Echer et al*., 2011a], but there are exceptions to this [*Tsurutani et al*., 1992a]. It is interesting to note that a few superstorms occurred during the descending phases of SCs 21 and 23.

Out of the 74 SSS events occurring during the period of study (1981 –2012), 46% were associated with intense geomagnetic storms, 49% with superstorms, 1% with moderate geomagnetic storms ($-50\,\text{nT} \geq Dst > -100\,\text{nT}$), and 4% occurred during geomagnetically quiet conditions ($Dst > -50\,\text{nT}$) (not shown).

We have also examined the SSS events from another perspective. The superstorms that occurred during 1981 to 2012 were analyzed to determine how often SSS events were related to these storm events. During this period, there were 24 superstorms, 15 (~63%) of which had associated SSS events. Thus, there is some relationship between SSS events and superstorms, but there is no one-to-one correspondence between the two phenomena. This topic will be discussed further later in the paper.

### 3.4. SSS Relationship With Geomagnetic Storm Phases

The magnetic storm phases during the SSS events were examined using high resolution *SYM-H* indices. The results are summarized in Table 2. The overwhelmed majority (86.5%) of the SSS events occurred in the main phase of geomagnetic storms. A few (9.5%) occurred in the recovery phase. Three SSS events took place when there was no geomagnetic storm ($SYM\text{-}H > -50\,\text{nT}$).

We grouped the SSS events according to the time lag between the SSS SML peaks and the storm *SYM-H* peaks. The events are then ordered in terms of the storm peak *SYM-H* onset, taken as the zero epoch time, $t = 0$. For each interval of time relative to $t = 0$, we calculated the *SYM-H* average values and their standard deviations. This is shown in Figure 4 (bottom).

**Table 2.** SSS Events During Different Geomagnetic Conditions

| Geomagnetic Condition | Number of SSSs | SSS (%) |
|---|---|---|
| Magnetic storm main phase | 64 | 86.5 |
| Magnetic storm recovery phase | 7 | 9.5 |
| Quiet time | 3 | 4 |

Figure 4 (top) shows the number of SSS events that occurred in particular time bins. It is observed that 28 SSSs (38% of all 74 events under study) occurred in the interval 0–2 h prior to geomagnetic storm peak. The highest occurrence rate (15 events,

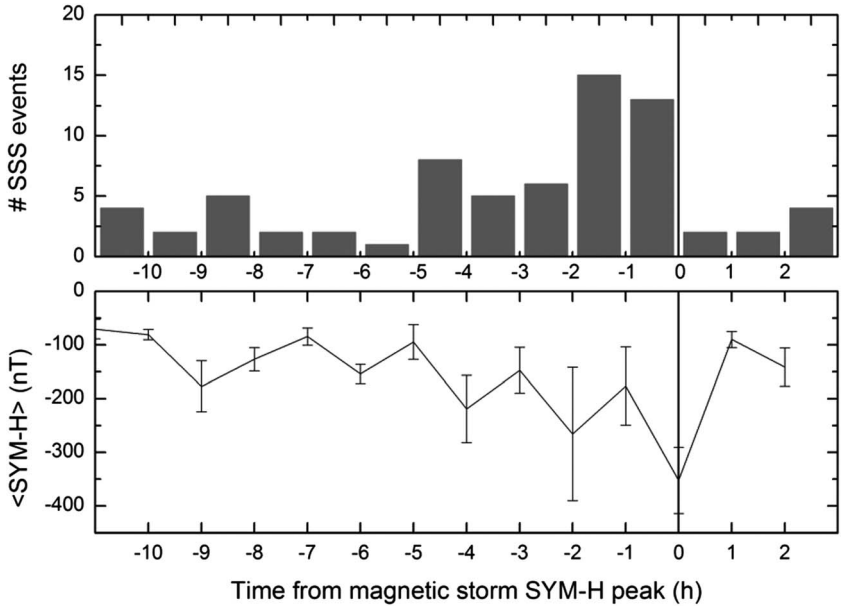


**Figure 4.** (top) The distribution of SSS events in time prior to or after magnetic storm peak intensity ($t = 0$) in histogram format. The vertical scale is the number of events. Time is given in hour from the *SYM-H* peak. (bottom) The average (solid line) and standard deviations (vertical bars) of the *SYM-H* values at each 1 h interval.

i.e., 20%) is found in the 1–2 h interval prior to the storm peak. The remainder of the SSS events occurred in either the storm main phase (47%) but $>$ 2 h before the peak *SYM-H*, the storm recovery phase (11%), or was not storm related at all (4%). The above results indicate that SSSs do not coincide with geomagnetic storm peaks. If we compare the data in Figure 4 (top and bottom), it can be noted that there is no obvious strong correspondence between *SYM-H* strength and SSS occurrence. This is shown below quantitatively in Figure 5.

Figure 5 shows the instantaneous *SYM-H* values at the peak of each SSS events (*SYM-H_s*) and peak *SYM-H* values of the geomagnetic storms (*SYM-H_p*) associated with the SSS events. The *SYM-H_s* and *SYM-H_p* values ranged from +54 to −562 nT and from −73 to −589 nT, respectively. The entire data set was binned into different values of *SYM-H_s* and *SYM-H_p* (Figure 5, first column). The SSS events are found to be

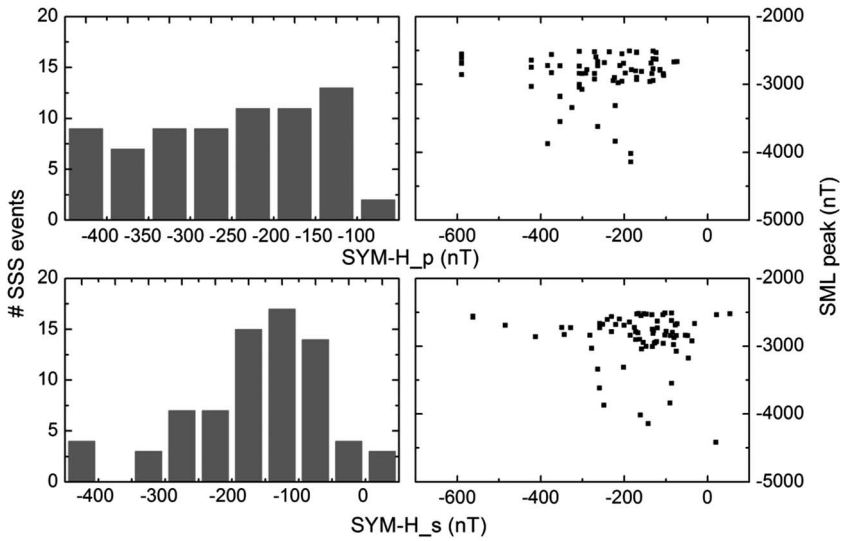


**Figure 5.** (first column) The SSS distributions (number of SSS events) for different ranges of peak *SYM-H* values (*SYM-H_p* in nT) and instantaneous *SYM-H* values at the time of SSS peaks (*SYM-H_s* in nT). (second column) The variations of SSS peak strength (SML peak in nT) as functions of *SYM-H_p* and *SYM-H_s*.

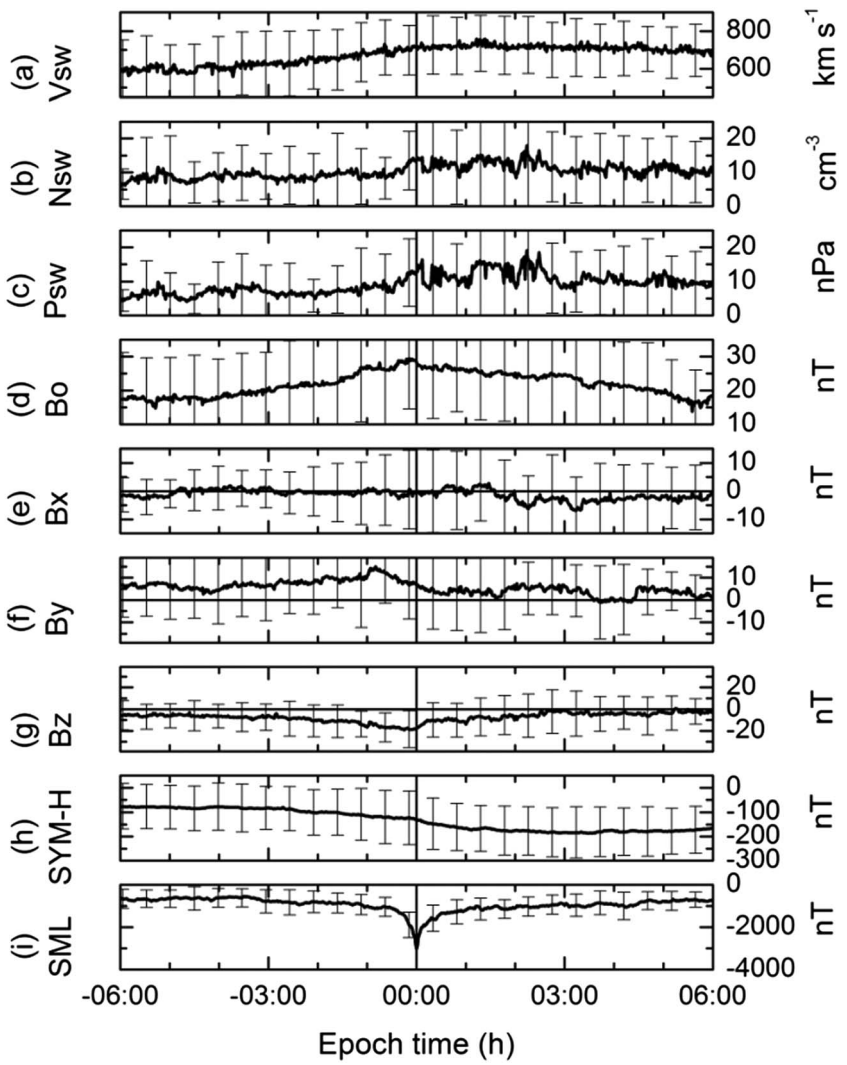


**Figure 6.** Superposed solar wind plasma variation during 24 isolated SSS events. From top to bottom, the panels show (a) $V_{sw}$ (km s$^{-1}$), (b) $N_{sw}$ (cm$^{-3}$), (c) $P_{sw}$ (nPa), (d) IMF $B_o$ (nT), (e) the $B_x$ (nT), (f) $B_y$ (nT) and (g) $B_z$ (nT) components in GSM coordinates, and (h) the *SYM-H* (nT) and (i) SML (nT) indices. The zero epoch time corresponds to the peak SML strength of the SSS events. The curves show the average values (1 min time resolution), while the vertical bars show the standard deviations at 30 min intervals.

distributed almost uniformly with respect to the *SYM-H_p*, while most (~62%) of the SSS events have instantaneous *SYM-H* values (*SYM-H_s*) in the range of −50 to −200 nT. In Figure 5 (second column), we plot the SSS strength (SML peak) against corresponding *SYM-H_p* and *SYM-H_s* values. These plots show that there is no obvious linear relationship between the SSS strength and *SYM-H_p* or *SYM-H_s*. In other words, SSS occurrence and SSS strength do not depend on the strength of associated geomagnetic storms.

### 3.5. SSS Superposed Epoch Analyses

During the recent complete solar cycle (SC 23), from 1996 to 2008, 37 SSS events were detected. Among them, 24 were isolated events which were separated by > 6 h from one another. The remaining 13 were separated by < 6 h. We analyzed the solar wind/interplanetary data for the 24 well-defined isolated SSS events. Earlier events were omitted because the interplanetary data were often either only low time resolution or were missing.

Figure 6 shows the results of the superposed epoch analysis of the solar wind/interplanetary plasma data. The parameters, from top to bottom panels, are the solar wind plasma speed ($V_{sw}$), the plasma density ($N_{sw}$), ram pressure ($P_{sw}$), IMF magnitude ($B_o$), and $B_x$, $B_y$, and $B_z$ components. Figures 6h and 6i show the geomagnetic

indices *SYM-H* and SML. The time corresponding to the SSS peak strength (SML peak) was taken as the zero epoch time ($t = 0$). The superposed averages at 1 min time resolution are shown by the solid curves, while vertical bars show the standard deviations ($1\sigma$) at 30 min intervals of time.

The average of all isolated SSS events shown in Figure 6i indicates that the SML profile smoothly decreases before the peak value and then smoothly increases after the peak value. The two isolated events shown in Figure 1 were similar in nature. This is the typical case for all SSS events studied. The average superposed SML value reached a peak of ~ −3030 nT. The average superposed peak *AL* value was ~ −2923 nT (not shown). This is for the 24 isolated SSSs occurring during SC 23. The highest SML strength during this period was −4418 nT (*AL* = −4046 nT). It may be noted that the average of SSS strength for all events during 1981–2012 period was ~ −2883 nT (*AL* = ~2849 nT).

The SML peak occurred in enhanced *SYM-H*, ~2 h before the *SYM-H* peak. This is consistent with the result depicted by Figure 4. The average *SYM-H* peak was ~ −180 nT.

The SSS events were related to enhanced solar wind density ($N_{sw}$) and ram pressure ($P_{sw}$) events, as was shown for the first SSS event of Figure 1. However, we note from the error bars of both panels that the statistical significance of this is somewhat low. The SSS peak occurs in the positive gradient of $V_{sw}$, increasing from ~620 km s$^{-1}$ at $t$ = ~−3 h to ~720 km s$^{-1}$ at the SSS peak ($t = 0$). The IMF $B_o$ increased from ~20 nT to ~30 nT during the same interval.

The expansion phase of the SSS was associated with the decrease of the IMF $B_z$. The IMF $B_z$ reached the minimum value of ~ −19 nT, ~15 min before the SSS peak. A prominent northward turning of $B_z$ leads the SML peak by ~6 min.

The IMF $B_x$ and $B_y$ components panels were shown to illustrate any heliospheric current sheet (HCS) [*Smith et al*., 1978] dependences, if present. There is no apparent relationship present in the figure. However, since there is both IMF switching from positive (negative $B_x$ values in GSM coordinates) to negative (positive GSM $B_x$ values) polarities and negative to positive polarities in the data, these might average out. We therefore looked at individual events to identify the HCS crossings with respect to the SSS events. We did not find any obvious relationship.

Among the 24 SSS events occurring in SC 23, we were able to identify the associated interplanetary structures for 22 events. It was found that ~77% of the SSSs were associated with small regions of very high density solar wind plasma parcels or pressure pulses impinging upon the magnetosphere. This is also apparent in the superposed study (Figure 6). This indicates possible plasma density control in the energy coupling during the SSS events [*Goodrich et al*., 1998; *Shue and Kamide*, 2001]. About 9% of the SSS events were associated with shocks (extreme and sudden pressure pulses), and ~14% of the events were associated with IMF directional changes.

There were intense southward IMF $B_s$ fields during the expansion phases of all 24 isolated SSS events in SC 23 (Figure 6g). It was found that MCs were the responsible interplanetary structure in 46% cases and sheath fields in 54% cases. This is roughly the same division for the interplanetary causes of intense geomagnetic storms [*Tsurutani et al*., 1988; *Echer et al*., 2008a]. The amount of time duration of the IMF $B_s$ prior to the SSS event varied from case to case.

## 4. Summary

This paper reports, for the first time, a detailed statistical study on extremely intense substorms called supersubstorms/SSSs with peak SML intensity $< -2500$ nT. Seventy-four SSS events occurring from 1981 to 2012, a ~3 solar cycle interval, were identified and analyzed using measurements from the SuperMAG network of ground-based magnetometers.

The main results of the present study may be summarized as follows:

1. The SSS events can occur during all phases of the solar cycle (Figure 3). The highest occurrence frequency was recorded in the solar cycle descending phase (3.8 year$^{-1}$), with a comparable occurrence rate during solar maximum (3.1 year$^{-1}$). The occurrence frequency was considerably lower in the ascending phase (1.5 year$^{-1}$) and the lowest at solar minimum (0.9 year$^{-1}$) (Table 1).

2. The number of SSS events showed an annual variation, with the maximum occurrence altering between spring equinox in SC 22 and fall equinox in SC 23 (Figure 2). Possible ionospheric control on the SSS occurrence was suggested.
3. The occurrence frequency as well as the strength of SSSs did not bear any obvious strong relationship with the strength of associated geomagnetic storms (Figure 5).
4. The SSS events were associated with southward IMFs provided by the sheath fields in 54% of the times and the magnetic clouds in 46% of the times.
5. About 77% of the SSSs were associated with small regions of very high density solar wind plasma parcels or pressure pulses impinging upon the magnetosphere.

There were no SSS events during the two solar/geomagnetic minima, 1996–1997, 2008–2009, and the neighboring years of the latter minimum, 2006–2007. The SSS events were often (but not always) found to be isolated peak occurrences in the SML indices. About 63% of the events had peak SML separated by $>6$ h, ~15% were separated by 1–6 h, and ~22% of the events were separated by $<1$ h from one another. For all the events under study, the average SML intensity was $-2883$ nT, with $-4418$ nT being the most intense event. Of the 74 SSS events, ~49% were associated with superstorms ($Dst \leq -250$ nT), 46% with intense geomagnetic storms ($-100\,\text{nT} \geq Dst > -250\,\text{nT}$), 1% with moderate geomagnetic storms ($-50\,\text{nT} > Dst \geq -100\,\text{nT}$), and 4% occurred during geomagnetically quiet ($Dst \geq -50$ nT). The majority (86.5%) of the SSS events occurred in the main phase of geomagnetic storms. About 9.5% occurred in the storm recovery phase.

## 5. Discussion and Conclusions

We have shown by individual example and superposed epoch analyses that the SSS events are isolated extremely intense substorm intervals. Our present results are consistent with *Tsurutani et al*. [2015]. In this paper we have presented results from a much larger sample with far more details of the SSS events and their energetics.

It is not surprising that SSS events are typically related to magnetic storms, but it is surprising that there is no one-to-one relationship to storm main phases or to storm peak intensities. The explanation to the latter feature is that large southward IMF $B_z$ associated with either the interplanetary magnetic clouds (46%) or the interplanetary sheath fields (54%) which leads to the SSS events (present study) also leads to the storms [*Tsurutani et al*., 1988; *Echer et al*., 2008b].

It has been noted that ground electrical anomalies [*Loomis*, 1861] occur during extreme magnetic storms such as for the September 1859 storm [*Carrington*, 1859; *Hodgson*, 1859; *Kimball*, 1960; *Tsurutani et al*., 2003b; *Lakhina and Tsurutani*, 2016] and the August 1972 event [*Anderson et al*., 1974; *Boteler and van Beek*, 1999; *Lanzerotti*, 1992; *Tsurutani et al*., 1992b, 2003b]. A major power outage occurred during the Hydro-Quebec 1989 storm [*Allen et al*., 1989; *Czech et al*., 1992; *Lakhina and Tsurutani*, 2016]. This strong focus on past extreme storms in the literature gives one the impression that magnetic storms are the cause of power outages at Earth. However, this impression is an oversimplification. It should be realized that what causes power outages is most likely associated with strong overhead ionospheric currents inducing very large $dB/dt$ currents in power transmission lines [*Tsurutani et al*., 2015]. These, of course, occur during SSS events, the focus of this paper. The SSSs that occur during geomagnetic storm main phases will have the advantage that the associated ionospheric currents will occur at lower latitudes due to the lower latitude location of the auroras and ionospheric currents. These lower latitudes will place the currents over highly populated regions.

*Huttunen et al*. [2008] have investigated geomagnetically induced currents (GICs) at the Mäntsälä station pipeline, Finland, located at ~56° to 58° magnetic latitude. They find only a loose correlation between GICs and magnetic storms during SC 23, similar to the relationship between SSSs and magnetic storms presented in the present paper. In fact, *Huttunen et al*. [2008] found that the most intense GICs are likely to take place during sheaths upstream of interplanetary coronal mass ejections rather than associated with magnetic cloud (MC) intervals. In contrast to the above arguments, we find here roughly half of SSS events are associated with sheath intervals and half with MC intervals. The *Tsurutani et al*. [2015] Figure 2 SSS events were MC events.

Further work is needed to better understand the relationship between SSS events and GICs. Can a strong correlation be found between the two so that eventual predictions can be made? Although this is beyond the scope of the present work, we encourage space weather researchers to make such studies.

**Acknowledgments**

The work of R.H. is financially supported by Fundação de Amparo à Pesquisa do Estado de São Paulo (FAPESP) through a postdoctoral research fellowship at INPE and by ANR under the financial agreement ANR-15-CE31-0009-01 at LPC2E/CNRS. E.E. would like to thank Brazilian CNPq (302583/2015-7) agency for financial support. Portions of this research were performed at the Jet Propulsion Laboratory, California Institute of Technology, under contract with NASA. The SuperMAG data were collected from the website: http://supermag.jhuapl.edu/. The solar wind/interplanetary data were collected from OMNI website: http://omniweb.gsfc.nasa.gov/. The geomagnetic indices we collected are from the World Data Center for Geomagnetism, Kyoto, Japan http://wdc.kugi.kyoto-u.ac.jp/, and the $F_{10.7}$ solar flux from http://www.drao.nrc.ca/icarus.

## References

Abraham-Schrauner, B. (1972), Determination of magnetohydrodynamic shock normals, *J. Geophys. Res.*, *77*, 736–739, doi:10.1029/JA077i004p00736.

Ahn, B. H., H. W. Kroehl, Y. Kamide, and E. A. Kihn (2000), Universal time variations of the auroral electrojet indices, *J. Geophys. Res.*, *105*, 267–275, doi:10.1029/1999JA900364.

Akasofu, S. I. (1964), The development of the auroral substorm, *Planet. Space Sci.*, *12*, 273–282, doi:10.1016/0032-0633(64)90151-5.

Akasofu, S. I. (1968), *Polar and Magnetospheric Substorms*, D. Reidel, Norwell, Mass.

Akasofu, S. I. (2004), Several "controversial" issues on substorms, *Space Sci. Rev.*, *113*, 1–40, doi:10.1023/B:SPAC.0000042938.57710.fb.

Allen, J., H. Sauer, L. Frank, and P. Reiff (1989), Effects of the March 1989 solar activity, *Eos Trans. AGU*, *70*, 1479–1488, doi:10.1029/89EO00409.

Anderson, C. W., L. J. Lanzerotti, and C. G. MacLennan (1974), Outage of the L4 system and the geomagnetic disturbances of 4 August 1972, *Bell Sys. Tech. J.*, *53*, 1817–1837, doi:10.1002/j.1538-7305.1974.tb02817.x.

Baker, D. N., T. I. Pulkkinen, V. Angelopoulos, W. Baumjohann, and R. L. McPherron (1996), Neutral line model of substorms: Past results and present view, *J. Geophys. Res.*, *101*, 12,975–13,010, doi:10.1029/95JA03753.

Beggan, C. D., D. Beamish, A. Richards, G. S. Kelly, and A. W. P. Thomson (2013), Prediction of extreme geomagnetically induced currents in the UK high-voltage network, *Space Weather*, *11*, 407–419, doi:10.1002/swe.20065.

Boteler, D. H., and G. J. van Beek (1999), August 4, 1972 revisited: A new look at the geomagnetic disturbance that caused the L4 cable system outage, *Geophys. Res. Lett.*, *26*, 577–580, doi:10.1029/1999GL900035.

Carrington, R. C. (1859), Description of a singular appearance seen in the Sun on September 1, 1859, *Mon. Not. R. Astron. Soc.*, *20*, 13–15, doi:10.1093/mnras/20.1.13.

Chakraborty, S. K., and R. Hajra (2010), Variability of total electron content near the crest of the equatorial anomaly during moderate geomagnetic storms, *J. Atmos. Sol. Terr. Phys.*, *72*, 900–911, doi:10.1016/j.jastp.2010.05.006.

Czech, P., S. Chano, H. Huynh, and A. Dutil (1992), The Hydro-Quebec system blackout of 13 March 1989: System response to geomagnetic disturbance, in *Proc. Geomagnetically Induced Currents Conference*, pp. 19.1–19.21, Millbrae, Calif.

Daglis, I. A., S. Livi, E. T. Sarris, and B. Wilken (1994), Energy density of ionospheric and solar wind origin ions in the near-Earth magnetotail during substorms, *J. Geophys. Res.*, *99*, 5691–5703, doi:10.1029/93JA02772.

Davis, T. N., and M. Sugiura (1966), Auroral electrojet activity index *AE* and its universal time variations, *J. Geophys. Res.*, *71*, 785–801, doi:10.1029/JZ071i003p00785.

Dungey, J. W. (1961), Interplanetary magnetic field and the auroral zones, *Phys. Rev. Lett.*, *6*, 47–48, doi:10.1103/PhysRevLett.6.47.

Echer, E., W. D. Gonzalez, B. T. Tsurutani, and A. L. C. Gonzalez (2008a), Interplanetary conditions causing intense geomagnetic storms ($Dst \leq -100$ nT) during solar cycle 23 (1996–2006), *J. Geophys. Res.*, *113*, A05221, doi:10.1029/2007JA012744.

Echer, E., W. D. Gonzalez, and B. T. Tsurutani (2008b), Interplanetary conditions leading to superintense geomagnetic storms ($Dst \leq -250$ nT) during solar cycle 23, *Geophys. Res. Lett.*, *35*, L06S03, doi:10.1029/2007GL031755.

Echer, E., W. D. Gonzalez, and B. T. Tsurutani (2011a), Statistical studies of geomagnetic storms with peak $Dst \leq -50$ nT from 1957 to 2008, *J. Atmos. Sol. Terr. Phys.*, *73*, 1454–1459, doi:10.1016/j.jastp.2011.04.021.

Echer, E., B. T. Tsurutani, W. D. Gonzalez, and J. U. Kozyra (2011b), High speed stream properties and related geomagnetic activity during the whole heliosphere interval (WHI): 20 March to April 2008, *Sol. Phys.*, *274*, 303–320, doi:10.1007/s11207-011-9739-0.

Echer, E., B. T. Tsurutani, and W. D. Gonzalez (2013), Interplanetary origins of moderate ($-100$ nT $< Dst \leq -50$ nT) geomagnetic storms during solar cycle 23 (1996–2008), *J. Geophys. Res. Space Physics*, *118*, 385–392, doi:10.1029/2012JA018086.

Gjerloev, J. W. (2009), A global ground-based magnetometer initiative, *Eos Trans. AGU*, *90*, 230–231, doi:10.1029/2009EO270002.

Gjerloev, J. W. (2012), The SuperMAG data processing technique, *J. Geophys. Res.*, *117*, A09213, doi:10.1029/2012JA017683.

Gonzalez, W. D., and B. T. Tsurutani (1987), Criteria of interplanetary parameters causing intense magnetic storms ($Dst < -100$ nT), *Planet. Space Sci.*, *35*, 1101–1109, doi:10.1016/0032-0633(87)90015-8.

Gonzalez, W. D., A. L. C. Gonzalez, and B. T. Tsurutani (1990), Dual peak solar cycle distribution of intense geomagnetic storms, *Planet. Space Sci.*, *38*, 181–187, doi:10.1016/0032-0633(90)90082-2.

Gonzalez, W. D., J. A. Joselyn, Y. Kamide, H. W. Kroehl, G. Rostoker, B. T. Tsurutani, and V. M. Vasyliunas (1994), What is a geomagnetic storm?, *J. Geophys. Res.*, *99*, 5771–5792, doi:10.1029/93JA02867.

Goodrich, C. C., J. G. Lyon, M. Wiltberger, R. E. Lopez, and K. Papadopou (1998), An overview of the impact of the January 10–11 1997 magnetic cloud on the magnetosphere via global MHD simulation, *Geophys. Res. Lett.*, *25*, 2537–2540, doi:10.1029/98GL01159.

Hajra, R. (2011), A study on the variability of total electron content near the crest of the equatorial anomaly in the Indian zone PhD thesis, Univ. of Calcutta, India.

Hajra, R., S. K. Chakraborty, and A. DasGupta (2010), Ionospheric effects near the magnetic equator and the anomaly crest of the Indian longitude zone during a large number of intense geomagnetic storms, *J. Atmos. Sol. Terr. Phys.*, *72*, 1299–1308, doi:10.1016/j.jastp.2010.09.015.

Hajra, R., E. Echer, B. T. Tsurutani, and W. D. Gonzalez (2013), Solar cycle dependence of high-intensity long-duration continuous *AE* activity (HILDCAA) events, relativistic electron predictors?, *J. Geophys. Res. Space. Physics*, *118*, 5626–5638, doi:10.1002/jgra.50530.

Hajra, R., E. Echer, B. T. Tsurutani, and W. D. Gonzalez (2014a), Solar wind-magnetosphere energy coupling efficiency and partitioning: HILDCAAs and preceding CIR storms during solar cycle 23, *J. Geophys. Res. Space. Physics*, *119*, 2675–2690, doi:10.1002/2013JA019646.

Hajra, R., E. Echer, B. T. Tsurutani, and W. D. Gonzalez (2014b), Superposed epoch analyses of HILDCAAs and their interplanetary drivers: Solar cycle and seasonal dependences, *J. Atmos. Sol. Terr. Phys.*, *121*, 24–31, doi:10.1016/j.jastp.2014.09.012.

Hajra, R., B. T. Tsurutani, E. Echer, and W. D. Gonzalez (2014c), Relativistic electron acceleration during high-intensity long-duration continuous *AE* activity (HILDCAA) events: Solar cycle phase dependences, *Geophys. Res. Lett.*, *41*, 1875–1881, doi:10.1002/2014GL059383.

Hajra, R., B. T. Tsurutani, E. Echer, W. D. Gonzalez, C. G. M. Brum, L. E. A. Vieira, and O. Santolik (2015a), Relativistic electron acceleration during HILDCAA events: Are precursor CIR magnetic storms important?, *Earth Planets Space*, *67*, 109, doi:10.1186/s40623-015-0280-5.

Hajra, R., B. T. Tsurutani, E. Echer, W. D. Gonzalez, and O. Santolik (2015b), Relativistic ($E > 0.6$, $> 2.0$ and $> 4.0$ MeV) electron acceleration at geosynchronous orbit during high-intensity long-duration continuous *AE* activity (HILDCAA) events, *Astrophys. J.*, *799*, 39–46, doi:10.1088/0004-637X/799/1/39.

Hamilton, D. C., G. Gloeckler, F. M. Ipavich, W. Studemann, B. Wilken, and G. Kremser (1988), Ring current development during the great geomagnetic storm of February 1986, *J. Geophys. Res.*, *93*, 14,343–14,355, doi:10.1029/JA093iA12p14343.
Hathaway, D. H. (2010), The solar cycle, *Living Rev. Sol. Phys.*, *7*, 1, doi:10.12942/lrsp-2010-1.
Hodgson, R. (1859), On a curious appearance seen in the Sun, *Mon. Not. R. Astron. Soc.*, *20*, 15–16, doi:10.1093/mnras/20.1.15a.
Huttunen, K. E. J., S. P. Kilpua, A. Pulkkinen, A. Viljanen, and E. Tanskanen (2008), Solar wind drivers of large geomagnetically induced currents during the solar cycle 23, *Space Weather*, *6*, S10002, doi:10.1029/2007SW000374.
Iyemori, T., and D. R. K. Rao (1996), Decay of the *Dst* field of geomagnetic disturbance after substorm onset and its implication to storm-substorm relation, *Ann. Geophys.*, *14*, 608–618, doi:10.1007/s00585-996-0608-3.
Kamide, Y., and S. I. Akasofu (1983), Notes on the auroral electrojet indices, *Rev. Geophys.*, *21*, 1647–1656, doi:10.1029/RG21i007p01647.
Kimball, D. S. (1960), A study of the aurora of 1859 Sci. Rpt. 6, UAG-R109, Univ. of Alaska, Fairbanks, Alaska.
Lakhina, G. S., and B. T. Tsurutani (2016), Geomagnetic storms: Historical perspective to modern view, *Geosci. Lett.*, *3*(1), 1–11, doi:10.1186/s40562-016-0037-4.
Lanzerotti, L. J. (1992), Comment on "Great magnetic storms" by Tsurutani et al., *Geophys. Res. Lett.*, *19*, 1991–1992, doi:10.1029/92GL02238.
Liou, K., P. T. Newell, D. G. Sibeck, C. I. Meng, M. Brittnacher, and G. Parks (2001), Observation of IMF and seasonal effects in the location of auroral substorm onset, *J. Geophys. Res.*, *106*, 5799–5810, doi:10.1029/2000JA003001.
Loomis, E. (1861), On the great auroral exhibition of Aug. 28th to Sept. 4, 1859, and on auroras generally, *Am. J. Sci.*, *82*, 318–335, doi:10.2475/ajs.s2-32.96.318.
Mursula, K., E. Tanskanen, and J. J. Love (2011), Spring-fall asymmetry of substorm strength, geomagnetic activity and solar wind: Implications for semiannual variation and solar hemispheric asymmetry, *Geophys. Res. Lett.*, *38*, L06104, doi:10.1029/2011GL046751.
Newell, P. T., and J. W. Gjerloev (2011a), Evaluation of SuperMAG auroral electrojet indices as indicators of substorms and auroral power, *J. Geophys. Res.*, *116*, A12211, doi:10.1029/2011JA016779.
Newell, P. T., and J. W. Gjerloev (2011b), Substorm and magnetosphere characteristic scales inferred from SuperMAG auroral electrojet indices, *J. Geophys. Res.*, *116*, A12232, doi:10.1029/2011JA016936.
Østgaard, N., N. A. Tsyganenko, S. B. Mende, H. U. Frey, T. J. Immel, M. Fillingim, L. A. Frank, and J. B. Sigwarth (2005), Observations and model predictions of substorm auroral asymmetries in the conjugate hemispheres, *Geophys. Res. Lett.*, *32*, L05111, doi:10.1029/2004GL022166.
Rostoker, G. (1972), Geomagnetic indices, *Rev. Geophys.*, *10*, 935–950, doi:10.1029/RG010i004p00935.
Rostoker, G., S. I. Akasofu, J. Foster, R. Greenwald, Y. Kamide, K. Kawasaki, A. Lui, R. McPherron, and C. Russell (1980), Magnetospheric substorms—Definition and signatures, *J. Geophys. Res.*, *85*, 1663–1668, doi:10.1029/JA085iA04p01663.
Schrijver, C. J., R. Dobbins, W. Murtagh, and S. M. Petrinec (2014), Assessing the impact of space weather on the electric power grid based on insurance claims for industrial electrical equipment, *Space Weather*, *12*, 487–498, doi:10.1002/2014SW001066.
Schwabe, H., and H. Schwabe (1844), Sonnenbeobachtungen im Jahre 1843, *Astron. Nachr.*, *21*, 234–235, doi:10.1002/asna.18440211505.
Shue, J. H., and Y. Kamide (2001), Effects of solar wind density on auroral electrojets, *Geophys. Res. Lett.*, *28*, 2181–2184, doi:10.1029/2000GL012858.
Smith, E. J. (1985), Interplanetary shock phenomena beyond 1 AU, in *Collisionless Shocks in the Heliosphere: Reviews of Current Research*, *Geophys. Monogr. Ser.*, vol. 35, edited by B. T. Tsurutani and R. G. Stone, 69 pp., AGU, Washington, D. C., doi:10.1029/GM035p0069.
Smith, E. J., B. T. Tsurutani, and R. L. Rosenberg (1978), Observations of the interplanetary sector structure up to heliographic latitudes of 16°: Pioneer 11, *J. Geophys. Res.*, *83*, 717–724, doi:10.1029/JA083iA02p00717.
Sugiura, M. (1980), What do we expect in magnetic activity in the current solar cycle?, *Eos Trans. AGU*, *61*, 673–675, doi:10.1029/EO061i043p00673.
Tsurutani, B. T., and W. D. Gonzalez (1987), The cause of high-intensity long-duration continuous *AE* activity (HILDCAAs): Interplanetary Alfvén wave trains, *Planet. Space Sci.*, *35*, 405–412, doi:10.1016/0032-0633(87)90097-3.
Tsurutani, B. T., and R. P. Lin (1985), Acceleration of $>$ 47 keV ions and $>$ 2 keV electrons by interplanetary shocks at 1 AU, *J. Geophys. Res.*, *90*, 1–11, doi:10.1029/JA090iA01p00001.
Tsurutani, B. T., and C. I. Meng (1972), Interplanetary magnetic-field variations and substorm activity, *J. Geophys. Res.*, *77*, 2964–2970, doi:10.1029/JA077i016p02964.
Tsurutani, B. T., W. D. Gonzalez, F. Tang, S. I. Akasofu, and E. J. Smith (1988), Origin of interplanetary southward magnetic fields responsible for major magnetic storms near solar maximum (1978–1979), *J. Geophys. Res.*, *93*, 8519–8531, doi:10.1029/JA093iA08p08519.
Tsurutani, B. T., W. D. Gonzalez, F. Tang, and Y. T. Lee (1992a), Great magnetic storms, *Geophys. Res. Lett.*, *19*, 73–76, doi:10.1029/91GL02783.
Tsurutani, B. T., W. D. Gonzalez, F. Tang, Y. T. Lee, M. Okada, and D. Park (1992b), Reply to L. J. Lanzerotti: Solar wind ram pressure corrections and an estimation of the efficiency of viscous interaction, *Geophys. Res. Lett.*, *19*, 1993–1994, doi:10.1029/92GL02239.
Tsurutani, B. T., X. Y. Zhou, and W. D. Gonzalez (2003a), A lack of substorm expansion phases during magnetic storms induced by magnetic clouds, in *Disturbances in Geospace: The Storm-Substorm Relationship*, edited by A. S. Sharma, Y. Kamide, and G. S. Lakhina, pp. 23–36, AGU, Washington, D. C., doi:10.1029/142GM03.
Tsurutani, B. T., W. D. Gonzalez, G. S. Lakhina, and S. Alex (2003b), The extreme magnetic storm of 1–2 September 1859, *J. Geophys. Res.*, *108*(A7), 1268, doi:10.1029/2002JA009504.
Tsurutani, B. T., W. D. Gonzalez, F. L. Guarnieri, Y. Kamide, X. Zhou, and J. K. Arballo (2004a), Are high-intensity long-duration continuous *AE* activity (HILDCAA) events substorm expansion events?, *J. Atmos. Sol. Terr. Phys.*, *66*, 167–176, doi:10.1016/j.jastp.2003.08.015.
Tsurutani, B. T., X. Zhou, W. D. Gonzalez, and F. L. Guarnieri (2004b), Substorms, auroral patches and quiet, The substorm-storm relationship during magnetic cloud induced storms, in *Substorms 7: Proc. 7th Inter. Conf. Subs.*, vol. 1, 63 pp., edited by N. Ganushkina and T. I. Pulkkinen, Finnish Meteorological Institute.
Tsurutani, B. T., G. S. Lakhina, O. P. Verkhoglyadova, W. D. Gonzalez, E. Echer, and F. L. Guarnieri (2011a), A review of interplanetary discontinuities and their geomagnetic effects, *J. Atmos. Sol. Terr. Phys.*, *73*, 5–19, doi:10.1016/j.jastp.2010.04.001.
Tsurutani, B. T., E. Echer, and W. D. Gonzalez (2011b), The solar and interplanetary causes of the recent minimum in geomagnetic activity (MGA23): A combination of midlatitude small coronal holes, low IMF $B_z$ variances, low solar wind speeds and low solar magnetic fields, *Ann. Geophys.*, *29*, 839–849, doi:10.5194/angeo-29-839-2011.
Tsurutani, B. T., R. Hajra, E. Echer, and J. W. Gjerloev (2015), Extremely intense (SML $\leq -2500$ nT) substorms: Isolated events that are externally triggered?, *Ann. Geophys. Commun.*, *33*, 519–524, doi:10.5194/angeo-33-519-2015.
Wang, H., and H. Lühr (2007), Seasonal-longitudinal variation of substorm occurrence frequency: Evidence for ionospheric control, *Geophys. Res. Lett.*, *34*, L07104, doi:10.1029/2007GL029423.
Zieger, B., and K. Mursula (1998), Annual variation in near-Earth solar wind speed: Evidence for persistent north-south asymmetry related to solar magnetic polarity, *Geophys. Res. Lett.*, *25*, 841–844, doi:10.1029/98GL50414.